Fixed-time leader-follower formation control of underactuated unmanned surface vehicles with unknown dynamics and ocean disturbances

Chenfeng Huang, Haitong Xu, Pedro Batista, Xianku Zhang, and C. Guedes Soares

European Journal of Control, vol. 70, 100784, March 2023

https://doi.org/10.1016/j.ejcon.2023.100784

Available online at www.sciencedirect.com

SciVerse ScienceDirect

European Journal of Control 00 (2012) 000–000

Fixed-time leader-follower formation control of underactuated unmanned surface vehicles with unknown dynamics and ocean disturbances

Chenfeng Huang[a,b], Haitong Xu[b], P. Batista[c], Xianku Zhang[a], C. Guedes Soares [b*]

[a]*Navigation College, Dalian Maritime University, 1 Linghai road, Dalian 116026, China*
[b]*Centre of Maritne Technology and Ocean Engineering (CENTEC), Instituto Superior Técnico, Universidade de Lisboa, Av. Rovisco Pais, Lisboa 1049-001, Portugal*
[c]*Institute for Systems and Robotics, LARSyS, Instituto Superior Técnico, Universidade de Lisboa, Av. Rovisco Pais, Lisboa 1049-001, Portugal*

Abstract

This paper investigates the formation control problem of underactuated unmanned surface vehicles with unknown dynamics and ocean disturbances. To tackle the leader-follower configuration, an improved fixed-time velocity controller is proposed for the virtual vehicle to guide the followers efficiently. For the tracking control of the follower vehicles, a concise controller is designed by borrowing backstepping and nonsingular sliding mode control techniques. A novel adaptive filter is developed to address the so-called "explosion of complexity" problem in the traditional backstepping framework, which could simplify the control structure and facilitate the implementation of the proposed controller in practical engineering. Furthermore, the radial basis function neural network is employed to identify the unknown dynamics of the vehicle model. A bounded-feedback adaptive law is developed to estimate the upper bound of ocean disturbances. That could greatly enhance the robustness and accuracy of the controller. Finally, a rigorous proof has been given to guarantee the practical fixed-time stability of the closed-loop system. Two examples are provided to demonstrate the effectiveness and superiority of the theoretical results.

Keywords: Underactuated vehicle; Leader-follower formation control; Fixed-time control; Neural network; Nonlinear sliding mode control

1. Introduction

In recent years, coordinated or cooperative control of multiple surface vehicles has been drawing great attention in the marine control community. Due to the increasing complexity of the marine environment, a single unmanned surface vehicle (USV) cannot accomplish maritime tasks even with sophisticated equipment[1-4]. Additionally, considering the economic cost and work efficiency, it is desirable to coordinate a

group of USVs to perform the tasks simultaneously. Compared with a single vehicle, the cooperative operation of multiple vehicles has some advantages, e.g. extensive sensing coverage[5-8], high fault tolerance[9-12], and strong robustness and adaptability[13,14]. Meanwhile, it has wide application prospects in the military and civil fields. Typical application scenarios include maritime patrol and surveillance, maritime search and rescue, naval convoy escort and marine resource exploration. To perform a cooperative operation, one fundamental idea is to achieve formation control of multiple vehicles whose objective is to maintain a desired geometric pattern such that the assigned task can be accomplished.

Currently, several effective approaches have been proposed to obtain the desired formation for multiple vehicles, e.g. behaviour-based control[15], virtual structures[16,17], leader-follower architecture[18,19], and topology-based control[20-22]. Among these, leader-follower architecture is preferred due to its simplicity and reliability in practical engineering. In such architecture, one or more leaders are introduced to track a time-varying path, then the followers are driven to their corresponding reference positions generated by the leader at different predefined ranges and bearings.

So far, significant results have been made in the leader-follower formation control of multiple vehicles. In [23], the leader-follower formation control of multiple nonholonomic mobile robots was investigated, and the formation architecture was obtained by fusion of the virtual vehicle guidance and trajectory tracking approach. In [24], an adaptive leader-follower controller was presented for a group of networked autonomous mobile robots, where a specific triangle formation is achieved without the need for neighbours' velocity. In [25], the authors studied the formation control problem of nonholonomic mobile robots, where the prescribed performance is guaranteed by the barrier Lyapunov function. In addition to the challenges in the aforementioned references, formation control of underactuated surface vehicles has the following inherent problems: (1) the dynamics of the vehicle are nonlinear and the accurate information of hydrodynamic terms is difficult to be determined; (2) the motion of the vehicle can be affected dramatically by the ocean disturbances, and (3) the underactuated model of the vehicle cannot be transformed into a driftless form and thus raise a unique challenge for controller design.

To overcome the challenges, a variety of leader-follower formation strategies have been developed for multiple underactuated surface vehicles[26,27]. Especially, neural networks (NNs) are universal approximators for smooth functions and thus are adopted by nonlinear controller design[28]. Considering the unknown leader dynamics and local dynamics, the problem of leader-follower formation control of underactuated surface vehicles was addressed by the introduction of NNs [29]. Using a similar approximation, a robust adaptive control scheme was designed for a group of marine surface vehicles, and the radial basis function neural network (RBFNN) related term was embedded into the controller to enhance the robustness of the closed-loop system in [30].

To cope with the adverse effect induced by the unknown plant parameters and ocean disturbances, Sun et al. presented a robust formation controller for USVs based on the PI sliding mode technique and parameter estimation approaches [31]. Lu et al. constructed an NN-based observer to estimate the ocean disturbances and then employ the minimum learning parameterization (MLP) technique to reduce the number of adaptive parameters [32]. The prescribed geometric formation with guaranteed transient performance for USVs was achieved via the transverse function and barrier Lyapunov function [33].

However, most of the aforementioned results focus on the asymptotic convergence or uniform ultimate bounds of the system performance. This means that all the states in the closed-loop system can reach the equilibrium point or its neighbourhood in infinite time, which is not able to meet the requirement of practical engineering. Despite some finite-time results that have been reported in [34, 35], the convergence time strictly

depends on the initial states of the system. Therefore, how to develop an effective control scheme for formation control of multiple underactuated USVs, such that the desired geometric formation can be achieved, and the fast convergence performance can be ensured, is a challenging topic that has not been addressed properly in the literature.

In this work, a novel fixed-time sliding mode controller is proposed for the formation control of underactuated USVs with unknown dynamics and ocean disturbances. To facilitate the leader-follower configuration, a virtual vehicle is introduced to guide the follower USVs to track the reference position. The RBFNNs are employed to address the unknown model uncertainty. The bounded-feedback adaptive law is developed to estimate the lumped disturbances which contain the upper bound of the approximation error of NNs and ocean disturbances. With the proposed algorithm, the formation tracking errors converge to a small residual set around the origin in a fixed time, the settling time is independent of the initial states of the system. The main contribution of the paper can be summarized as follows:

(1) An improved fixed-time velocity controller is presented for virtual vehicles to implement the tracking control of followers. In comparison with the conventional guidance principle[27] the presented algorithm possesses faster and more accurate guidance.
(2) A robust adaptive sliding mode control law is developed for the follower USVs. By fusing the RBFNNs and the bounded-feedback techniques, both the unknown high-order hydrodynamic terms of the USV and the lumped disturbances are identified and compensated. That could greatly enhance the robustness and improve the accuracy of the control strategy.
(3) A novel adaptive fixed-time filter is constructed to avoid the repeated derivative of the virtual controller, which could dramatically simplify the structure of the control strategy and thus facilitate the implementation of the controller in practical engineering.

The rest of this paper is organized as follows. In Section 2, some preliminaries and lemmas are provided. Then, the problem formulation of leader-follower formation control is presented. In Section 3, the adaptive velocity controller is designated for the virtual vehicle. Moreover, the fixed-time sliding mode controller is presented for the follower USV. Practical fixed-time stability of the closed-loop signals is proved based on Lyapunov theory. Section 4 shows the numerical simulation result of the proposed algorithm. Finally, Section 5 concludes the paper.

2. Background and problem formulation

2.1. Mathematical model of the underactuated USV

In this paper, the kinematic model of the USV can be described as

$$\dot{\boldsymbol{\eta}} = R(\psi)\boldsymbol{\upsilon} \tag{1}$$

where $\boldsymbol{\eta} = [x, y, \psi]^{\mathrm{T}} \in \mathbb{R}^3$ denotes the position vector in the inertial frame, x, y, ψ denote the position and yaw angle of the USV respectively, $\boldsymbol{\upsilon} = [u, v, r]^{\mathrm{T}}$ denotes the velocity vector in the body-fixed frame, u, v, r denote the surge velocity, sway velocity and yaw angle velocity, respectively. $R(\psi)$ is the rotation matrix with the form of

$$R(\psi) = \begin{bmatrix} \cos\psi & -\sin\psi & 0 \\ \sin\psi & \cos\psi & 0 \\ 0 & 0 & 1 \end{bmatrix}$$

The kinetics of the underactuated USV can be described as follows

$$\begin{cases} \dot{u} = \dfrac{m_v}{m_u} vr - \dfrac{1}{m_u} f_u(u) + \dfrac{1}{m_u}\tau_u + d_{wu} \\ \dot{v} = -\dfrac{m_u}{m_v} ur - \dfrac{1}{m_v} f_v(v) + d_{wv} \\ \dot{r} = \dfrac{m_u - m_v}{m_v} uv - \dfrac{1}{m_r} f_r(r) + \dfrac{1}{m_r}\tau_r + d_{wr} \end{cases} \tag{2}$$

with

$$f_u(u) = d_u u + d_{u_2}|u|u + d_{u_3}u^3$$
$$f_v(v) = d_v v + d_{v_2}|v|v + d_{v_3}v^3$$
$$f_r(r) = d_r r + d_{r_2}|r|r + d_{r_3}r^3$$

where m_u, m_v, m_r are inertia parameters, τ_u, τ_r are control inputs in surge and yaw directions respectively, d_{wu}, d_{wv}, d_{wr} are ocean disturbances induced by the wind, wave, and water currents, and $f_u(u), f_v(v), f_r(r)$ are nonlinear functions with hydrodynamic damping terms and nonlinear damping terms $d_u, d_{u_2}, d_{u_3}, d_v, d_{v_2}, d_{v_3}, d_r, d_{r_2}, d_{r_3}$.

For the leader-follower configuration, the leader is introduced to generate the reference position of the follower. The position vector of the leader USV is defined as $\boldsymbol{\eta_L} = [x_L, y_L, \psi_L]^{\mathrm{T}}$, the velocity vector is defined as $\boldsymbol{\upsilon_L} = [u_L, v_L, r_L]^{\mathrm{T}}$, the bearing angle between the leader and the follower is denoted as λ, and the distance between the leader and the follower is denoted as $\rho = \sqrt{(x_L - x)^2 + (y_L - y)^2}$.

Assumption 1. [36] The sway velocity of the underactuated USV is passive-bounded. Meanwhile, the velocity vector $\boldsymbol{\upsilon_L}$ of the leader is bounded by the unknown constant υ_M .

Assumption 2. The ocean disturbances d_{wu}, d_{wv}, d_{wr} are bounded by positive unknown constants $\bar{d}_{wu}, \bar{d}_{wv}, \bar{d}_{wr}$, such that $|d_{wu}| \le \bar{d}_{wu}, |d_{wv}| \le \bar{d}_{wv}, |d_{wr}| \le \bar{d}_{wr}$.

Remark 1. Since the USV motion in the sway direction is dominated and damped out by the hydrodynamics damping force, the sway dynamics is passively bounded. This assumption is consistent with marine practice and has been systematically analyzed by considering different cases [36].

2.2. Neural networks approximation

Function approximation is a technique for estimating unknown underlying functions using historical or available observations from the domain. Due to the excellent approximation ability and simple structure, the RBFNN is recognized as one of the best solutions for nonlinear approximation. In this paper, the RBFNN is employed to approximate the unknown part of the USV model. The detailed mathematical model of the RBFNN is illustrated as Lemma 1.

Lemma 1. [37, 38] Consider a continuous function $f(\boldsymbol{x})$ with $f(\boldsymbol{0}) = 0$, where $\boldsymbol{x}$ is defined in a compact set Ω_x . The RBFNN can be utilized to approximate the nonlinear function $f(\boldsymbol{x})$ as follows

$$f(\boldsymbol{x}) = \boldsymbol{W}^{\mathrm{T}}\varphi(\boldsymbol{x}) + \varepsilon, \quad \forall \boldsymbol{x} \in \Omega_x \tag{3}$$

where $\boldsymbol{W} \in \mathbb{R}^{\kappa \times 1}$ denotes the weight of the RBFNN, ε denotes the unknown constant approximation error with $\varepsilon \le \bar{\varepsilon}$, $\bar{\varepsilon}$ denotes the supremum of the approximation error, $\boldsymbol{\varphi}(\boldsymbol{x}) = \left[\varphi_1(\boldsymbol{x}), \varphi_2(\boldsymbol{x}), \ldots \varphi_\kappa(\boldsymbol{x})\right]^{\mathrm{T}}$ denotes the RBF vector with the form of Gaussian function

$$\varphi_i(\boldsymbol{x}) = \exp\left(-\frac{(x-\mu_i)^{\mathrm{T}}(x-\mu_i)}{2\varsigma_i^2}\right), i = 1, 2\cdots, \kappa \tag{4}$$

where ς_i denotes the width of the Gaussian function, μ_i denotes the centre of the receptive field, and $i = 1, 2, \ldots, \kappa$ denotes the number of neurons.

2.3. Other important definitions and lemmas

To facilitate the controller design in subsequent steps, some important definitions and lemmas are introduced as follows.

Definition 1. Consider the dynamical system with the following form

$$\dot{\boldsymbol{x}}(t) = f(t, \boldsymbol{x}), \ \boldsymbol{x}(0) = \boldsymbol{x}_0 \tag{5}$$

where $\boldsymbol{x} \in \mathbb{R}^n$ denotes the state of the system, $\boldsymbol{x}_0$ denotes the origin (equilibrium point) of the system, $f(\cdot): U_0 \to \mathbb{R}^n$ denotes a continuous function in an open neighbourhood U_0 of the origin $\boldsymbol{x}_0$. If the origin $\boldsymbol{x}_0$ of the system (5) is stable based on the Lyapunov function, then the fixed-time stability is defined as follows.

Lemma 2.[39] Consider the dynamical system (5), and suppose that there exists a positive definite Lyapunov function $V(\boldsymbol{x})$ such that

$$\dot{V}(\boldsymbol{x}) \le -aV(\boldsymbol{x})^p - bV(\boldsymbol{x})^q + \delta \tag{6}$$

where $a, b, \delta \in (0, \infty)$, $p \in (0,1)$, $q \in (1, \infty)$. Then the origin $\boldsymbol{x}_0$ of the system is practical fixed-time stable. Furthermore, the residual set of the solution of system (5) can be determined by

$$\left\{\lim_{t \to T} \boldsymbol{x}(t) \,|\, V(\boldsymbol{x}(t)) \le \min\left\{a^{-\frac{1}{p}}\left(\frac{\delta}{1-\mu}\right)^{\frac{1}{p}}, b^{-\frac{1}{q}}\left(\frac{\delta}{1-\mu}\right)^{\frac{1}{q}}\right\}\right\} \tag{7}$$

where $\mu \in (0,1)$. The convergence time satisfies

$$T \le T_{\max} := \frac{1}{a\mu(1-p)} + \frac{1}{b\mu(q-1)} \tag{8}$$

Lemma 3.[40] For any $\sigma > 0$ and $\omega \in \mathbb{R}$, the following inequality holds

$$0 \le |\omega| - \omega \tanh\left(\frac{\omega}{\sigma}\right) \le k_s \sigma \tag{9}$$

where k_s is a constant and satisfies $k_s = e^{-(k_s+1)}$, i.e. $k_s = 0.2758$.

Lemma 3.[41] For $\theta, \vartheta \in \mathbb{R}$ and any real numbers $\alpha > 0, \beta < 0, \varpi > 0$, the following inequality holds

$$|\theta|^\alpha |\vartheta|^\beta \le \frac{\alpha}{\alpha+\beta}\varpi|\theta|^{\alpha+\beta} + \frac{\beta}{\alpha+\beta}\varpi^{-\frac{p}{q}}|\vartheta|^{\alpha+\beta} \tag{10}$$

Lemma 4.[42] For $\lambda > 0$ and $\gamma_1 \ge 0, \gamma_2 > 0$, the following inequality holds

$$\gamma_1^\lambda(\gamma_2 - \gamma_1) \le \frac{1}{1+\lambda} \le \left(\gamma_2^{1+\lambda} - \gamma_1^{1+\lambda}\right) \tag{11}$$

Lemma 5.[43] For $\lambda > 0$ and $\gamma_1 \geq 0, \gamma_2 \leq \gamma_1$ and $\gamma_2 \in \mathbb{R}$, the following inequality holds

$$(\gamma_1 - \gamma_2)^{\lambda} \geq \gamma_2^{\lambda} - \gamma_1^{\lambda} \tag{12}$$

Lemma 6.[44] For any constants $s_1 > 0, s_2 > 0, s_3 > 0$ and $x, y \in \mathbb{R}$, the following inequality holds

$$|x|^{s_1} |y|^{s_2} \leq \frac{s_1}{s_1 + s_2} s_3 |x|^{s_1 + s_2} + \frac{s_2}{s_1 + s_2} s_3^{-\frac{s_1}{s_2}} \tag{13}$$

2.4. Problem statement

Consider a group of underactuated USVs, numbered from 1 to N, where each USV is subject to kinematic (1) and kinetics (2). Among these USVs, one of them is defined as a leader, and the rest are followers. By coordinating the range and bearings between the leader and followers, the desired formation of the USVs can be achieved. The objective of this paper is to design a sliding mode controller for followers with the consideration of model uncertainty and ocean disturbances, such that followers are capable to form and maintain the desired formation with the leader in a fixed-time.

3. Leader-follower formation control

To facilitate the formation configuration, the leader-follower structure is divided into leader USV-virtual vehicle structure and virtual vehicle-follower USV structure. As shown in Fig.1, the leader-follower formation control of multiple USVs can be achieved in 2 subsections: first, a fixed-time velocity controller is presented for virtual vessels to track reference positions generated by the leader USV. Second, a novel practical fixed-time sliding mode controller is designated for the follower USVs to track virtual vehicles.

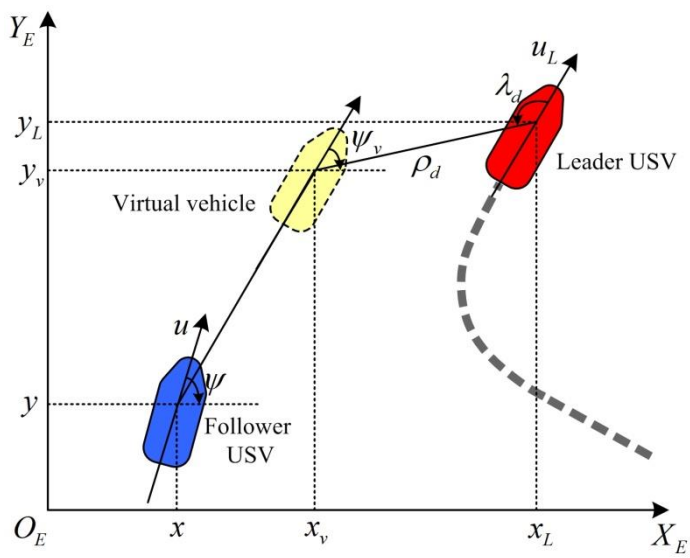

Fig.1 Schematic diagram of leader-follower configuration

3.1. Formation setup

In this subsection, to make the virtual vehicle track the reference position quickly, a kind of controller is presented to regulate the velocity of virtual vehicles based on [32]. For the formation configuration, the reference position is determined by the leader USV with desired distance ρ_d and bearing angle λ_d. Both the leader USV and virtual vehicles are subject to the ship's kinematic system and their motion can be described by

$$\dot{\boldsymbol{\eta}}_L = R(\psi_L)\boldsymbol{\upsilon}_L, \quad \dot{\boldsymbol{\eta}}_v = R(\psi_v)\boldsymbol{\upsilon}_v \tag{14}$$

where $\boldsymbol{\eta}_v = [x_v, y_v, \psi_v]^{\mathrm{T}}$ and $\boldsymbol{\upsilon}_v = [u_v, v_v, r_v]^{\mathrm{T}}$ denote the position vector and velocity vector of the virtual vehicle respectively. Then, the kinematic of the reference position can be derived as

$$\boldsymbol{\eta}_r = \boldsymbol{\eta}_L + R(\psi_L)\boldsymbol{l} \tag{15}$$

where $\boldsymbol{l} = [\rho_d \cos(\lambda_d), \rho_d \sin(\lambda_d), 0]^{\mathrm{T}}$ denotes the desired offset vector.

Define the error vector $\boldsymbol{\eta}_e = [e_1, e_2, e_3]^{\mathrm{T}}$ between the reference position and its corresponding virtual vehicle, i.e.,

$$\boldsymbol{\eta}_e = \boldsymbol{\eta}_r - \boldsymbol{\eta}_v \tag{16}$$

To guarantee the virtual vehicle is capable of tracking the reference position in a fixed-time, an adaptive controller is presented as

$$\boldsymbol{\upsilon}_v = R^{\mathrm{T}}(\psi_v)\left(K_1 \mathrm{sig}^p(\boldsymbol{\eta}_e) + K_2 \mathrm{sig}^q(\boldsymbol{\eta}_e) + \hat{\upsilon}_M \tanh\left(\frac{\boldsymbol{\eta}_e}{\sigma_\eta}\right)\right) \tag{17}$$

$$\dot{\hat{\upsilon}}_M = \chi_1\left(\boldsymbol{\eta}_e^{\mathrm{T}} \tanh\left(\frac{\boldsymbol{\eta}_e}{\sigma_\eta}\right) - k_3\hat{\upsilon}_M - k_4\hat{\upsilon}_M^q\right) \tag{18}$$

where $K_1, K_2 \in \mathbb{R}^{3\times 3}$ are positive define design matrices, $k_3, k_4, \chi_1 > 0$ are design parameters, $\mathrm{sig}^k(\cdot) = \mathrm{sign}(\cdot)|\cdot|^k$. $\hat{\upsilon}_M$ denotes the estimation value of υ_M, and $\tilde{\upsilon}_M = \upsilon_M - \hat{\upsilon}_M$, where $\upsilon_M \geq \boldsymbol{\upsilon}_L$ based on Assumption 1.

Consider the following Lyapunov candidate function $V_1 = 1/2\boldsymbol{\eta}_e^{\mathrm{T}}\boldsymbol{\eta}_e + 1/(2\chi_1)\tilde{\upsilon}_M^2$, taking the time derivative yields

$$\dot{V}_1 = \boldsymbol{\eta}_e^{\mathrm{T}}\dot{\boldsymbol{\eta}}_e - \frac{1}{\chi_1}\tilde{\upsilon}_M\dot{\hat{\upsilon}}_M \tag{19}$$

Substituting (14), (16), (17) into $\boldsymbol{\eta}_e^{\mathrm{T}}\dot{\boldsymbol{\eta}}_e$ gives

$$\begin{aligned}\boldsymbol{\eta}_e^{\mathrm{T}}\dot{\boldsymbol{\eta}}_e &= \boldsymbol{\eta}_e^{\mathrm{T}}\left(R(\psi_L)\boldsymbol{\upsilon}_L - R(\psi_v)\boldsymbol{\upsilon}_v\right)\\ &= \boldsymbol{\eta}_e^{\mathrm{T}}\left(R(\psi_L)\boldsymbol{\upsilon}_L - R(\psi_v)R^{\mathrm{T}}(\psi_v)\left(K_1 \mathrm{sig}^p(\boldsymbol{\eta}_e) + K_2 \mathrm{sig}^q(\boldsymbol{\eta}_e) + \hat{\upsilon}_M \tanh\left(\frac{\boldsymbol{\eta}_e}{\sigma_\eta}\right)\right)\right)\\ &\leq \|\boldsymbol{\eta}_e^{\mathrm{T}}\|\upsilon_M - \lambda_{\min}(K_1)\|\boldsymbol{\eta}_e\|^{p+1} - \lambda_{\min}(K_2)\|\boldsymbol{\eta}_e\|^{q+1} - \boldsymbol{\eta}_e^{\mathrm{T}}\hat{\upsilon}_M \tanh\left(\frac{\boldsymbol{\eta}_e}{\sigma_\eta}\right)\end{aligned} \tag{20}$$

Substituting (18) into $\tilde{\upsilon}_M\dot{\hat{\upsilon}}_M/\chi_1$, leads to

$$\begin{aligned}\frac{1}{\chi_1}\tilde{\upsilon}_M\dot{\tilde{\upsilon}}_M &= \tilde{\upsilon}_M\left(\boldsymbol{\eta}_e^{\mathrm{T}}\tanh\left(\frac{\boldsymbol{\eta}_e}{\sigma_\eta}\right)-k_3\hat{\upsilon}_M-k_4\hat{\upsilon}_M^q\right)\\ &= \tilde{\upsilon}_M\boldsymbol{\eta}_e^{\mathrm{T}}\tanh\left(\frac{\boldsymbol{\eta}_e}{\sigma_\eta}\right)-k_3\hat{\upsilon}_M\tilde{\upsilon}_M-k_4\hat{\upsilon}_M^q\tilde{\upsilon}_M\end{aligned} \tag{21}$$

According to (20), (21) and Lemma 3, the following inequality can be derived

$$\begin{aligned}\dot{V}_1 &\le \left\|\boldsymbol{\eta}_e^{\mathrm{T}}\right\|\upsilon_M-\lambda_{\min}\left(K_1\right)\left\|\boldsymbol{\eta}_e\right\|^{p+1}-\lambda_{\min}\left(K_2\right)\left\|\boldsymbol{\eta}_e\right\|^{q+1}-\hat{\upsilon}_M\boldsymbol{\eta}_e^{\mathrm{T}}\tanh\left(\frac{\boldsymbol{\eta}_e}{\sigma_\eta}\right)\\ &-\tilde{\upsilon}_M\boldsymbol{\eta}_e^{\mathrm{T}}\tanh\left(\frac{\boldsymbol{\eta}_e}{\sigma_\eta}\right)+k_3\hat{\upsilon}_M\tilde{\upsilon}_M+k_4\hat{\upsilon}_M^q\tilde{\upsilon}_M\\ &\le -\lambda_{\min}\left(K_1\right)\left\|\boldsymbol{\eta}_e\right\|^{p+1}-\lambda_{\min}\left(K_2\right)\left\|\boldsymbol{\eta}_e\right\|^{q+1}+k_3\hat{\upsilon}_M\tilde{\upsilon}_M+k_4\hat{\upsilon}_M^q\tilde{\upsilon}_M+k_s\sigma_\eta\upsilon_M\end{aligned} \tag{22}$$

Based on Lemma 4 and Lemma 5, then

$$\begin{aligned}\hat{\upsilon}_M^q\tilde{\upsilon}_M &= \hat{\upsilon}_M^q\left(\upsilon_M-\hat{\upsilon}_M\right)\\ &\le \frac{1}{1+q}\left(\upsilon_M^{1+q}-\hat{\upsilon}_M^{1+q}\right)\\ &= \frac{1}{1+q}\left(\upsilon_M^{1+q}-\left(\upsilon_M-\tilde{\upsilon}_M\right)^{1+q}\right)\\ &\le \frac{1}{1+q}\left(2\upsilon_M^{1+q}-\tilde{\upsilon}_M^{1+q}\right)\end{aligned} \tag{23}$$

Therefore, by adding and subtracting the term $k_3\left(\tilde{\upsilon}_M^2/2\right)^{(p+1)/2}$, (22) can be rewritten as

$$\begin{aligned}\dot{V}_1 &\le -\lambda_{\min}\left(K_1\right)\left\|\boldsymbol{\eta}_e\right\|^{p+1}-\lambda_{\min}\left(K_2\right)\left\|\boldsymbol{\eta}_e\right\|^{q+1}-\frac{k_4}{1+q}\tilde{\upsilon}_M^{1+q}+\frac{2k_4}{1+q}\upsilon_M^{1+q}\\ &-\frac{k_3}{2}\tilde{\upsilon}_M^2+\frac{k_3}{2}\upsilon_M^2+k_s\sigma_\eta\upsilon_M-k_3\left(\frac{\tilde{\upsilon}_M^2}{2}\right)^{\frac{p+1}{2}}+k_3\left(\frac{\tilde{\upsilon}_M^2}{2}\right)^{\frac{p+1}{2}}\end{aligned} \tag{24}$$

Using Lemma 6, let $x=\tilde{\upsilon}_M^2/2, y=1, s_1=(p+1)/2, s_2=(1-p)/2, s_3=2/(p+1)$, and the term $k_3\left(\tilde{\upsilon}_M^2/2\right)^{(p+1)/2}$ can be transformed into

$$k_3\left(\frac{\tilde{\upsilon}_M^2}{2}\right)^{\frac{p+1}{2}} \le k_3\frac{\tilde{\upsilon}_M^2}{2}+\frac{1-p}{2}k_3\left(\frac{p+1}{2}\right)^{\frac{p+1}{1-p}} \tag{25}$$

Then, one has

$$\dot{V}_1 \le -\lambda_{\min}\left(K_1\right)\left\|\boldsymbol{\eta}_e\right\|^{p+1}-\lambda_{\min}\left(K_2\right)\left\|\boldsymbol{\eta}_e\right\|^{q+1}-k_3\left(\frac{\tilde{\upsilon}_M^2}{2}\right)^{\frac{p+1}{2}}-\frac{k_4}{1+q}\tilde{\upsilon}_M^{1+q}+\delta_1 \tag{26}$$

where $\delta_1=\left(2k_4/(1+q)\right)\upsilon_M^{1+q}+\left(k_3/2\right)\upsilon_M^2+k_s\sigma_\eta\upsilon_M+\left((1-p)k_3/2\right)\left((p+1)/2\right)^{(p+1)/(1-p)}$.

Remark 2. Actually, for a certain follower, only the leader information is required to complete the formation configuration. No information from neighbouring followers is needed to develop the formation control strategy. Besides, the information of the leader is obtained by the followers indirectly: the virtual vehicle is

introduced to transfer the information from leader to followers and facilitate the path tracking of followers.

3.2. Formation tracking control

This subsection proposes a novel fixed-time sliding mode controller for the follower USVs. The design process consists of two steps (see Fig.2). In the first step, the virtual controller is designed for the kinematic system of the follower USV. Meanwhile, to avoid the problem of "explosion of complexity" occurring in conventional backstepping frameworks, an adaptive fixed-time filter is constructed to estimate the derivative of the virtual controller. In the second step, the RBFNN is employed to estimate the model uncertainty. An adaptive fixed-time sliding mode controller is developed for the kinetic system of the follower USV. The detailed process of the controller design is illustrated as follows.

Step 1. Define the tracking errors between the virtual vehicle and the follower USV as

$$\begin{bmatrix} x_e \\ y_e \\ \psi_e \end{bmatrix} = R(\psi)^{\mathrm{T}} \begin{bmatrix} x_v - x \\ y_v - y \\ \psi_v - \psi \end{bmatrix} \tag{27}$$

The time derivative of (27) is

$$\begin{aligned} \dot{x}_e &= -u + u_v \cos\psi_e + r y_e \\ \dot{y}_e &= -v + u_v \sin\psi_e - r x_e \\ \dot{\psi}_e &= -r + r_v \end{aligned} \tag{28}$$

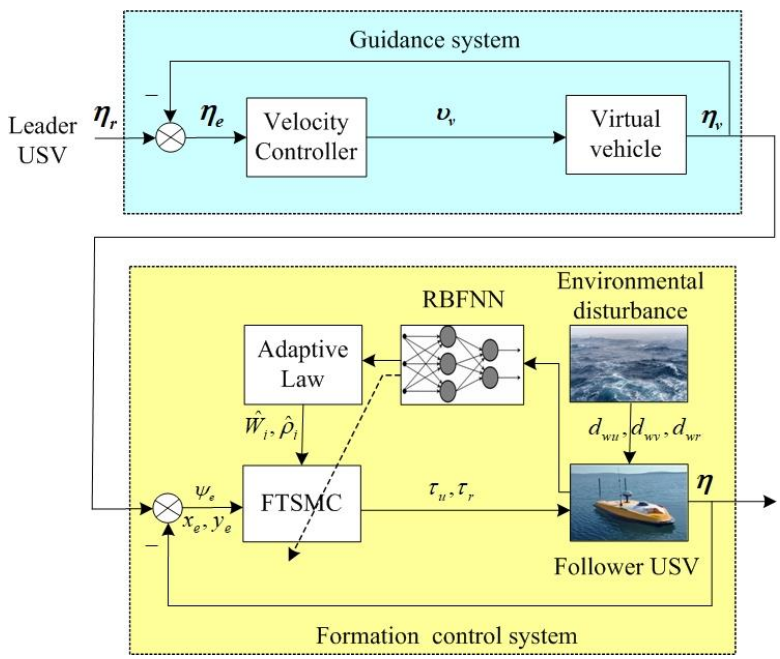

Fig.2 Block diagram of the fixed-time leader-follower control

For u, ψ_e, select the corresponding virtual controllers $\alpha_u, \alpha_{\psi_e}$ as

$$\begin{aligned}\alpha_u &= k_{x_1}\mathrm{sig}^p\left(x_e\right)+k_{x_2}\mathrm{sig}^q\left(x_e\right)+u_v\cos\psi_e,\\ \alpha_{\psi_e} &= \mathrm{atan}\left(\frac{-k_{y_1}\mathrm{sig}^p\left(y_e\right)-k_{y_2}\mathrm{sig}^q\left(y_e\right)+v}{u_v}\right)\end{aligned} \tag{29}$$

where $k_{x_1},k_{x_2},k_{y_1},k_{y_2}>0$ are the design parameters. Then $\dot{x}_e,\dot{y}_e$ in (28) can be written as

$$\begin{aligned}\dot{x}_e &= -\alpha_u+u_v\cos\psi_e+ry_e\\ \dot{y}_e &= -v+u_v\sin\alpha_{\psi_e}-rx_e\end{aligned} \tag{30}$$

Furthermore, to avoid repeated differentiation of virtual control laws α_u,α_{ψ_e} in the subsequent design, a fixed-time filter is constructed as

$$\begin{aligned}t_i\dot{\beta}_i &= \mathrm{sig}^p\left(\xi_i\right)+\xi_i^q+t_i\hat{\zeta}_i\tanh\left(\frac{\hat{\zeta}_i\xi_i}{\sigma_i}\right)\\ \dot{\hat{\zeta}}_i &= -k_{\xi_{1i}}\hat{\zeta}_i-k_{\xi_{2i}}\hat{\zeta}_i^q+\xi_i,\quad i=u,\psi_e\end{aligned} \tag{31}$$

where $\sigma_i,k_{\xi_{1i}},k_{\xi_{2i}}>0$ are all design parameters, t_i denotes the time constant, β_i denotes the filtered signal of α_i, $\xi_i=\alpha_i-\beta_i$ denotes the filtered error, and $\beta_i\left(0\right)=\alpha_i\left(0\right)$. $\zeta_i\ge\left|\dot{\alpha}_i\right|$ denotes an unknown constant, $\hat{\zeta}_i$ denotes the estimation of ζ_i, and $\tilde{\zeta}_i=\zeta_i-\hat{\zeta}_i$.

Since β_{ψ_e} cannot be directly involved in the controller design of step 2. We further introduce α_r to stabilize ψ_e. For subsystem $\dot{\psi}_e$ in (28), the corresponding virtual controller α_r is designated as

$$\alpha_r = k_{\psi_1}\mathrm{sig}^p\left(\psi_e\right)+k_{\psi_2}\mathrm{sig}^q\left(\psi_e\right)+r_v \tag{32}$$

where $k_{\psi_1},k_{\psi_2}>0$ are the design parameters. Meanwhile, the filter (31) is also utilized, with $\xi_r=\alpha_r-\beta_r$ and $\zeta_r\ge\left|\dot{\alpha}_r\right|$, where β_r is the filtered signal of α_r, and $\beta_r\left(0\right)=\alpha_r\left(0\right)$.

Select the Lyapunov candidate function $V_2=x_e^2/2+y_e^2/2+\psi_e^2/2$. Its time derivative is given by

$$\dot{V}_2 = x_e\dot{x}_e+y_e\dot{y}_e+\psi_e\dot{\psi}_e \tag{33}$$

In light of (29), (31), (32), one obtains

$$\begin{aligned}x_e\dot{x}_e &= x_e\left(-\alpha_u+u_v\cos\psi_e+ry_e\right)\\ &= x_e\left(-k_{x_1}\mathrm{sig}^p\left(x_e\right)-k_{x_2}\mathrm{sig}^q\left(x_e\right)+ry_e\right)\\ &\le -k_{x_1}\left|x_e\right|^{p+1}-k_{x_2}\left|x_e\right|^{q+1}+rx_ey_e\end{aligned} \tag{34}$$

$$\begin{aligned}y_e\dot{y}_e &= y_e\left(-v+u_v\sin\alpha_{\psi_e}-rx_e\right)\\ &= y_e\left(-k_{y_1}\mathrm{sig}^p\left(y_e\right)-k_{y_2}\mathrm{sig}^q\left(y_e\right)-rx_e\right)\\ &\le -k_{y_1}\left|y_e\right|^{p+1}-k_{y_2}\left|y_e\right|^{q+1}-rx_ey_e\end{aligned} \tag{35}$$

$$\begin{aligned}\psi_e\dot{\psi}_e &= \psi_e\left(r_v-r\right)\\ &= \psi_e\left(-k_{\psi_1}\mathrm{sig}^p\left(\psi_e\right)-k_{\psi_2}\mathrm{sig}^q\left(\psi_e\right)\right)\\ &\le -k_{\psi_1}\left|\psi_e\right|^{p+1}-k_{\psi_2}\left|\psi_e\right|^{q+1}\end{aligned} \tag{36}$$

Substituting (34), (35), (36) into (33) gives

$$\dot{V}_2 \le -k_{x_1}\left|x_e\right|^{p+1} - k_{x_2}\left|x_e\right|^{q+1} - k_{y_1}\left|y_e\right|^{p+1} - k_{y_2}\left|y_e\right|^{q+1} - k_{\psi_1}\left|\psi_e\right|^{p+1} - k_{\psi_2}\left|\psi_e\right|^{q+1} \tag{37}$$

Consider the Lyapunov candidate function $V_{3i} = \xi_i^2/2 + \tilde{\zeta}_i^2/2,\ i = u, r, \psi_e$, taking the time derivative of V_{3i}, the following inequality can be obtained based on (31),

$$\begin{aligned}
\dot{V}_{3i} &= \xi_i\dot{\xi}_i + \tilde{\zeta}_i\dot{\tilde{\zeta}}_i \\
&= \xi_i\left(\dot{\alpha}_i - \dot{\beta}_i\right) - \tilde{\zeta}_i\dot{\hat{\zeta}}_i \\
&\le \xi_i\zeta_i - \frac{1}{t_i}\left|\xi_i\right|^{p+1} - \frac{1}{t_i}\left|\xi_i\right|^{q+1} - \xi_i\hat{\zeta}_i\tanh\left(\frac{\hat{\zeta}_i\xi_i}{\sigma_i}\right) + k_{\xi_{1i}}\tilde{\zeta}_i\hat{\zeta}_i + k_{\xi_{2i}}\tilde{\zeta}_i\hat{\zeta}_i^q - \left|\xi_i\right|\tilde{\zeta}_i \\
&\le -\frac{1}{t_i}\left|\xi_i\right|^{p+1} - \frac{1}{t_i}\left|\xi_i\right|^{q+1} + k_{\xi_{1i}}\tilde{\zeta}_i\hat{\zeta}_i + k_{\xi_{2i}}\tilde{\zeta}_i\hat{\zeta}_i^q + k_s\sigma_i
\end{aligned} \tag{38}$$

Similarly to the derivation of (24), (25), (26), by adding and subtracting the term $k_{\xi_{1i}}\left(\tilde{\zeta}_i^2/2\right)^{(p+1)/2}$, it can be readily shown that

$$\begin{aligned}
\dot{V}_{3i} &\le -\frac{1}{t_i}\left|\xi_i\right|^{p+1} - \frac{1}{t_i}\left|\xi_i\right|^{q+1} + k_s\sigma_i - \frac{1}{2}k_{\xi_{1i}}\tilde{\zeta}_i^2 + \frac{1}{2}k_{\xi_{1i}}\zeta_i^2 - \frac{k_{\xi_{2i}}}{q+1}\tilde{\zeta}_i^{q+1} + \frac{2k_{\xi_{2i}}}{q+1}\zeta_i^{q+1} \\
&\le -\frac{1}{t_i}\left|\xi_i\right|^{p+1} - \frac{1}{t_i}\left|\xi_i\right|^{q+1} - k_{\xi_{1i}}\left(\frac{\tilde{\zeta}_i^2}{2}\right)^{\frac{p+1}{2}} - \frac{k_{\xi_{2i}}}{q+1}\tilde{\zeta}_i^{q+1} + \delta_{3i}
\end{aligned} \tag{39}$$

where $\delta_{3i} = \left(k_{\xi_{1i}}/2\right)\zeta_i^2 + \left(2k_{\xi_{2i}}/(q+1)\right)\zeta_i^{q+1} + k_s\sigma_i + \left((1-p)k_{\xi_{1i}}/2\right)\left((p+1)/2\right)^{(p+1)/(1-p)}$.

Step 2. Define the kinetic error as $u_e = u - \beta_u$, $r_e = r - \beta_r$. Taking the time derivative of u_e, r_e based on (2), it is possible to derive

$$\begin{aligned}
\dot{u}_e &= F_u\left(\cdot\right) + \frac{1}{m_u}\tau_u + d_{wu} - \dot{\beta}_u \\
\dot{r}_e &= F_r\left(\cdot\right) + \frac{1}{m_r}\tau_r + d_{wr} - \dot{\beta}_r
\end{aligned} \tag{40}$$

where $F_u\left(\cdot\right) = m_v vr/m_u - f_u\left(u\right)/m_u$, $F_r\left(\cdot\right) = \left(m_u - m_v\right)uv/m_v - f_r\left(r\right)/m_r$. By Lemma l, the RBFNN is utilized to estimate the model uncertainty $F_u\left(\cdot\right), F_r\left(\cdot\right)$, and (40) can be rewritten as

$$\dot{i}_e = W_i^{\mathrm{T}}\varphi\left(\upsilon\right) + \varepsilon_i + \frac{1}{m_i}\tau_i + d_{wi} - \dot{\beta}_i,\ i = u, r \tag{41}$$

Next, following the design of [41], a fixed-time terminal sliding mode (FTTSM) is constructed based on function $\phi_i\left(i_e\right),\ i = u, r$.

$$S_i = i_e + \gamma_i\phi\left(i_e\right),\ i = u, r \tag{42}$$

where $\phi_i\left(i_e\right) = \mathrm{sig}\left(i_e\right)^p + \mathrm{sig}\left(i_e\right)^q$ and $\gamma_i > 0$ is a design parameter.

To stabilize the kinetic error, a fixed-time sliding mode controller is developed as

$$\tau_i = m_i\left(-k_{i1}\mathrm{sig}(S_i)^p - k_{i2}\mathrm{sig}(S_i)^q - \hat{W}_i^T\varphi(\upsilon) - \hat{\rho}_i\mathrm{sign}(S_i) + \dot{\beta}_i - \gamma_i\dot{\phi}_i\right),\ i = u, r \tag{43}$$

where $k_{i1}, k_{i2} > 0$ are design parameters, $\hat{W}_i$ denotes the estimation value of W_i, and $\tilde{W}_i = W_i - \hat{W}_i$. Moreover, $\rho_i = \bar{\varepsilon}_i + \bar{d}_{wi}$ denotes the lumped disturbance, $\hat{\rho}_i$ denotes the estimation value of ρ_i, and $\tilde{\rho}_i = \rho_i - \hat{\rho}_i$. The adaptive law is selected as

$$\begin{aligned}\dot{\hat{W}}_i &= \Gamma_{i1}\varphi(\upsilon)S_i\\ \dot{\hat{\rho}}_i &= \Gamma_{i2}|S_i|,\ i = u, r\end{aligned} \tag{44}$$

where $\Gamma_{i1}, \Gamma_{i2} > 0$ are the design parameters.

Consider the Lyapunov candidate function $V_{4i} = 1/2S_i^2$, $i = u, r$. Taking the time derivative of V_{4i}, one obtains

$$\dot{V}_{4i} = S_i\dot{S}_i \tag{45}$$

According to (41), (42), (43)

$$\begin{aligned}S_i\dot{S}_i &= S_i\left(\dot{i}_e + \gamma_i\dot{\phi}(i_e)\right)\\ &\le S_i\left(W_i^{\mathrm{T}}\varphi(\upsilon) + \bar{\varepsilon}_i + \frac{1}{m_i}\tau_i + \bar{d}_{wi} - \dot{\beta}_i + \gamma_i\dot{\phi}(i_e)\right)\\ &= S_i\left(W_i^{\mathrm{T}}\varphi(\upsilon) - k_{i1}\mathrm{sig}(S_i)^p - k_{i2}\mathrm{sig}(S_i)^q - \hat{W}_i^T\varphi(\upsilon) - \hat{\rho}_i\mathrm{sign}(S_i) + \rho_i\right)\\ &\le -k_{i1}|S_i|^{p+1} - k_{i2}|S_i|^{q+1} + S_i\tilde{W}_i^{\mathrm{T}}\varphi(\upsilon) + |S_i|\tilde{\rho}_i\end{aligned} \tag{46}$$

Then,

$$\dot{V}_{4i} \le -k_{i1}|S_i|^{p+1} - k_{i2}|S_i|^{q+1} + S_i\tilde{W}_i^{\mathrm{T}}\varphi(\upsilon) + |S_i|\tilde{\rho}_i \tag{47}$$

Select the Lyapunov candidate function $V_{pi} = 1/2\,\mathrm{Tr}\left[\tilde{W}_i^{\mathrm{T}}\Gamma_{i1}^{-1}\tilde{W}_i\right] + 1/2\,\Gamma_{i2}^{-1}\tilde{\rho}_i^2$, $i = u, r$, taking the time derivative of V_{pi}, leads to

$$\dot{V}_{pi} = -\tilde{W}_i^{\mathrm{T}}\Gamma_{i1}^{-1}\dot{\hat{W}}_i - \Gamma_{i2}^{-1}\tilde{\rho}_i\dot{\hat{\rho}}_i \tag{48}$$

Based on (44), (48)

$$\begin{aligned}-\tilde{W}_i^{\mathrm{T}}\Gamma_{i1}^{-1}\dot{\hat{W}}_i &= -\tilde{W}_i^{\mathrm{T}}\varphi(\upsilon)S_i\\ -\Gamma_{i2}^{-1}\tilde{\rho}_i\dot{\hat{\rho}}_i &= -\tilde{\rho}_i|S_i|\end{aligned} \tag{49}$$

Substituting (49) into (48) and simplifying it yields

$$\dot{V}_{pi} = -\tilde{W}_i^{\mathrm{T}}\varphi_i(\upsilon)S_i - \tilde{\rho}_i|S_i| \tag{50}$$

Remark 3. Except for the fixed-time convergence, small computational burdern is another merit of the proposed controller. Benefiting from the constructed adaptive filter, the complexity of the controller structure is greatly reduced, which leads to smaller computational burden and thus facilitates the implementation of the algorithm in practical engineering.

3.3. Main result

Theorem 1. Consider the leader-follower formation control of follower USVs (1), (2) with Assumptions 1 and 2. Consider the velocity controller (17) of the virtual vehicle and the velocity estimation law (18), the virtual

control law (29), (32), the fixed-time filter (31) and the fixed-time sliding mode control law (43), the adaptive law (44). Then, the signals $\boldsymbol{\eta_e}, \tilde{\upsilon}_M, x_e, y_e, \psi_e, \xi_u, \xi_r, \xi_{\psi_e}, \tilde{\zeta}_u, \tilde{\zeta}_r, \tilde{\zeta}_{\psi_e}, S_u, S_r$ in the closed-loop system are satisfied as practical fixed-time stability.

Proof: The overall Lyapunov candidate function is given as $V_o = V_1 + V_2 + \sum_{i=u,r,\psi_e} V_{3i} + \sum_{i=u,r} V_{4i} + \sum_{i=u,r} V_{pi}$. It follows that

$$\begin{aligned}\dot{V}_o \le & -\lambda_{\min}\left(K_1\right)\left\|\boldsymbol{\eta_e}\right\|^{p+1} - \lambda_{\min}\left(K_2\right)\left\|\boldsymbol{\eta_e}\right\|^{q+1} - k_3\left(\frac{\tilde{\upsilon}_M^2}{2}\right)^{\frac{p+1}{2}} - \frac{k_4}{1+q}\tilde{\upsilon}_M^{1+q} \\ & - k_{x_1}\left|x_e\right|^{p+1} - k_{x_2}\left|x_e\right|^{q+1} - k_{y_1}\left|y_e\right|^{p+1} - k_{y_2}\left|y_e\right|^{q+1} - k_{\psi_1}\left|\psi_e\right|^{p+1} - k_{\psi_2}\left|\psi_e\right|^{q+1} \\ & - \sum_{i=u,r,\psi_e}\left(\frac{1}{t_i}\left|\xi_i\right|^{p+1} + \frac{1}{t_i}\left|\xi_i\right|^{q+1} + k_{\xi_{1i}}\left(\frac{\tilde{\zeta}_i^2}{2}\right)^{\frac{p+1}{2}} + \frac{k_{\xi_{2i}}}{q+1}\tilde{\zeta}_i^{q+1}\right) \\ & - k_{i1}\left|S_i\right|^{p+1} - k_{i2}\left|S_i\right|^{q+1} + \delta\end{aligned} \tag{51}$$

where $\delta = \delta_1 + \sum_{i=u,r,\psi_e}\delta_{3i}$. (51) implies that for any initial conditions $\boldsymbol{\eta_e}(0), \tilde{\upsilon}_M(0), x_e(0), y_e(0), \psi_e(0), \xi_u(0), \xi_r(0), \xi_{\psi_e}(0), \tilde{\zeta}_u(0), \tilde{\zeta}_r(0), \tilde{\zeta}_{\psi_e}(0), S_u(0), S_r(0), \tilde{W}_u(0), \tilde{W}_r(0), \tilde{\rho}_u(0), \tilde{\rho}_r(0)$, we can adjust the design parameters $K_1, K_2, k_3, k_4, k_{x_1}, k_{x_2}, k_{y_1}, k_{y_2}, k_{\psi_1}, k_{\psi_2}, k_{\xi_{1i}}, k_{\xi_{2i}}, k_{i1}, k_{i2}$ such that all signals in the closed-loop system are uniform and ultimately bounded.

Based on the above conclusion, assume that there exist positive constants $\left|S_i\right| \le \sigma_{Si}$, $\left\|\tilde{W}_i\right\|_F \le \sigma_{0i}$, $\left|\tilde{\rho}_i\right| \le \sigma_{1i}$. Since $0 < \varphi(\boldsymbol{\upsilon}) \le 1$ holds for all neurons $i = 1, 2\cdots, \kappa$, then $\left\|\varphi_i(\boldsymbol{\upsilon})\right\| \le \sqrt{\kappa}$ as $\varphi(\boldsymbol{\upsilon}) = \left[\varphi_1(\boldsymbol{\upsilon}), \varphi_2(\boldsymbol{\upsilon}), \ldots \varphi_\kappa(\boldsymbol{\upsilon})\right]^{\mathrm{T}}$. Then, the following inequality can be obtained

$$\left\|\tilde{W}_i^{\mathrm{T}}\varphi(\boldsymbol{\upsilon})\right\|_F \le \left\|\tilde{W}_i^{\mathrm{T}}\right\|_F \left\|\varphi(\boldsymbol{\upsilon})\right\| = \sqrt{\kappa}\sigma_{0i} \tag{52}$$

Define $\sigma_{2i} = \sqrt{\kappa}\sigma_{0i}$ and $\sigma_{3i} = \sigma_{1i} + \sigma_{2i}$. It follows from (47) that

$$\begin{aligned}\dot{V}_{4i} &\le -k_{i1}\left|S_i\right|^{p+1} - k_{i2}\left|S_i\right|^{q+1} + \sqrt{\kappa}\sigma_{0i}\left|S_i\right| + \sigma_{1i}\left|S_i\right| \\ &= -k_{i1}\left|S_i\right|^{p+1} - k_{i2}\left|S_i\right|^{q+1} + \sigma_{3i}\left|S_i\right| \\ &\le -k_{i1}2^{\frac{p+1}{2}}\left(\frac{1}{2}S_i^2\right)^{\frac{p+1}{2}} - k_{i2}2^{\frac{q+1}{2}}\left(\frac{1}{2}S_i^2\right)^{\frac{q+1}{2}} + \sigma_{3i}2^{\frac{1}{2}}\left(\frac{1}{2}S_i^2\right)^{\frac{1}{2}} \\ &= -\gamma_{i1}V_{4i}^{\frac{p+1}{2}} - \gamma_{i2}V_{4i}^{\frac{q+1}{2}} + \gamma_{i3}V_{4i}^{\frac{1}{2}}\end{aligned} \tag{53}$$

where $\gamma_{i1} = k_{i1}2^{(p+1)/2}$, $\gamma_{i2} = k_{i2}2^{(q+1)/2}$, $\gamma_{i3} = \sigma_{3i}2^{1/2}$. To eliminate the third term in (53), one considers $\gamma_{i1} = \gamma_{i1}^a + \gamma_{i1}^b$ such that

$$\left|S_i\right| \ge \delta_{Si} = \sqrt{2}\left(\frac{\gamma_{i3}}{\gamma_{i1}^b}\right)^{\frac{1}{p}} \tag{54}$$

Then, (53) can be transformed into

$$\dot{V}_{4i} \le -\gamma_{i1}^a V_{4i}^{\frac{p+1}{2}} - \gamma_{i2}V_{4i}^{\frac{q+1}{2}} \tag{55}$$

Consider the Lyapunov candidate function $V = V_1 + V_2 + \sum_{i=u,r,\psi_e} V_{3i} + \sum_{i=u,r} V_{4i}$. From (51) and (55), one obtains

$$\begin{aligned}\dot{V} \le & -2^{\frac{p+1}{2}}\lambda_{\min}(K_1)\left(\frac{1}{2}\|\boldsymbol{\eta}_e\|^2\right)^{\frac{p+1}{2}} - 2^{\frac{q+1}{2}}\lambda_{\min}(K_2)\left(\frac{1}{2}\|\boldsymbol{\eta}_e\|^2\right)^{q+1} - k_3\left(\frac{\tilde{\upsilon}_M^2}{2}\right)^{\frac{p+1}{2}} - 2^{\frac{q+1}{2}}\frac{k_4}{1+q}\left(\frac{1}{2}\tilde{\upsilon}_M^2\right)^{\frac{q+1}{2}} \\ & - 2^{\frac{p+1}{2}}k_{x_1}\left(\frac{1}{2}|x_e|^2\right)^{p+1} - 2^{\frac{q+1}{2}}k_{x_2}\left(\frac{1}{2}|x_e|^2\right)^{q+1} - 2^{\frac{p+1}{2}}k_{y_1}\left(\frac{1}{2}|y_e|^2\right)^{\frac{p+1}{2}} - 2^{\frac{q+1}{2}}k_{y_2}\left(\frac{1}{2}|y_e|^2\right)^{\frac{q+1}{2}} \\ & - 2^{\frac{p+1}{2}}k_{\psi_1}\left(\frac{1}{2}|\psi_e|^2\right)^{\frac{p+1}{2}} - 2^{\frac{q+1}{2}}k_{\psi_2}\left(\frac{1}{2}|\psi_e|^2\right)^{\frac{q+1}{2}} - \sum_{i=u,r,\psi_e}\left(2^{\frac{p+1}{2}}\frac{1}{t_i}\left(\frac{1}{2}|\xi_i|^2\right)^{\frac{p+1}{2}} + 2^{\frac{q+1}{2}}\frac{1}{t_i}\left(\frac{1}{2}|\xi_i|^2\right)^{\frac{q+1}{2}}\right) \\ & - \sum_{i=u,r,\psi_e}\left(k_{\xi_{1i}}\left(\frac{\tilde{\zeta}_i^2}{2}\right)^{\frac{p+1}{2}} + 2^{\frac{q+1}{2}}\frac{k_{\xi_{2i}}}{q+1}\left(\frac{1}{2}\tilde{\zeta}_i^2\right)^{\frac{q+1}{2}}\right) - \sum_{i=u,r}\left(\gamma_{i1}^a\left(\frac{1}{2}S_i^2\right)^{\frac{p+1}{2}} + \gamma_{i2}\left(\frac{1}{2}S_i^2\right)^{\frac{q+1}{2}}\right) + \delta\end{aligned} \tag{56}$$

To prove the practical fixed-time stability of the signals $\boldsymbol{\eta}_e, \tilde{\upsilon}_M, x_e, y_e, \psi_e, \xi_u, \xi_r, \xi_{\psi_e}, \tilde{\zeta}_u, \tilde{\zeta}_r, \tilde{\zeta}_{\psi_e}, S_u, S_r$, the design parameters should be adjusted appropriately such that

$$\begin{aligned}&\gamma_{\eta 1} = 2^{\frac{p+1}{2}}\lambda_{\min}(K_1),\ \ \gamma_{\eta 2} = 2^{\frac{q+1}{2}}\lambda_{\min}(K_2),\ \ \gamma_{\upsilon 1} = k_3,\ \ \gamma_{\upsilon 2} = 2^{\frac{q+1}{2}}\frac{k_4}{1+q}, \\ &\gamma_{x1} = 2^{\frac{p+1}{2}}k_{x_1},\ \ \gamma_{x2} = 2^{\frac{q+1}{2}}k_{x_2},\ \ \gamma_{y1} = 2^{\frac{p+1}{2}}k_{y_1},\ \ \gamma_{y2} = 2^{\frac{q+1}{2}}k_{y_2},\ \ \gamma_{\psi 1} = 2^{\frac{p+1}{2}}k_{\psi_1}, \\ &\gamma_{\psi 2} = 2^{\frac{q+1}{2}}k_{\psi_2},\ \ \gamma_{\xi 1}^i = 2^{\frac{p+1}{2}}\frac{1}{t_i},\ \ \gamma_{\xi 2}^i = 2^{\frac{q+1}{2}}\frac{1}{t_i},\ \ \gamma_{\zeta 1}^i = k_{\xi_{1i}},\ \ \gamma_{\zeta 2}^i = 2^{\frac{q+1}{2}}\frac{k_{\xi_{2i}}}{q+1}.\end{aligned}$$

Therefore

$$\dot{V} \le -\gamma_1 V^{\frac{p+1}{2}} - \gamma_2 V^{\frac{q+1}{2}} + \delta \tag{57}$$

where $\gamma_1 = \min\left\{\gamma_{\eta 1}, \gamma_{\upsilon 1}, \gamma_{x1}, \gamma_{y1}, \gamma_{\psi 1}, \gamma_{\xi 1}^i, \gamma_{\zeta 1}^i, \gamma_{i1}^a\right\}, \gamma_2 = \min\left\{\gamma_{\eta 2}, \gamma_{\upsilon 2}, \gamma_{x2}, \gamma_{y2}, \gamma_{y2}, \gamma_{\xi 2}^i, \gamma_{\zeta 2}^i, \gamma_{I2}\right\}$.

According to Lemma 2, it can be inferred that the signals $\boldsymbol{\eta}_e, \tilde{\upsilon}_M, x_e, y_e, \tilde{\psi}_e, \xi_u, \xi_r, \xi_{\psi_e}, \tilde{\zeta}_u, \tilde{\zeta}_r, \tilde{\zeta}_{\psi_e}, S_u, S_r$ in the leader-follower formation closed-loop system are practical fixed-time stable. Moreover, all the aforementioned signals will converge into a small residual set $D_1 = \left\{V \middle| V \le \min\left\{\left(\gamma_1^{-1/p}\left(\delta/(1-\mu)\right)\right)^{1/p}, \left(\gamma_2^{-1/q}\left(\delta/(1-\mu)\right)\right)^{1/q}\right\}\right\}$ around the origin, the convergence time can be estimated by $T_s \le T_{\max} = 1/\gamma_1\left(\mu(1-p)\right) + 1/\gamma_2\left(\mu(1-q)\right)$.

Remark 4. It is noticed that although it seems there are many control parameters to be determined to satisfy (57), only a few of them have a dominant influence on the closed-loop performance, e.g., $K_1, K_2, k_{x_1}, k_{x_2}, k_{y_1}, k_{y_2}$. Most of the remaining parameters have little impact on the system performance. For the dominant control parameters, we can determine them by tuning the value while observing the response of the simulation result. Too much or too small control parameters will lead to undesired performance, e.g., overshot, or slow divergence. Then, it is not difficult to narrow down the selection range of potential value and achieve the optimal control parameters.

4. Numerical simulation

In this section, numerical simulations are performed to demonstrate the effectiveness and superiority of the proposed control law. Model uncertainty and ocean disturbances are considered to verify the closed-loop performance of the pentagon formation control in Section 4.1. Then, a comparison simulation with the existing result in [32] is performed to further verify the proposed controller by a single pair leader-follower in Section 4.2. For the simulation, the identical follower USV with a length of 32 m and mass of 118×10^3 kg is selected as the control plant. The detailed parameters include added mass and damping matrices of the follower USVs, as given by $m_u=120\times10^3\text{kg}$, $m_v=177.9\times10^3\text{kg}$, $m_r=636\times10^3\text{kg}\cdot\text{m}^2$, $d_u=215\times10^2\text{kg}\cdot\text{s}^{-1}$, $d_v=117\times10^3\text{kg}\cdot\text{s}^{-1}$, $d_r=802\times10^4\text{kg}\cdot\text{m}^2\cdot\text{s}^{-1}$. As for the leader, the initial states are set as $\boldsymbol{\eta}_L=[0\text{m},0\text{m},\pi/12\text{rad}]^{\mathrm{T}}$, $\boldsymbol{\upsilon}_L=[0\text{m/s},0\text{m/s},0\text{rad/s}]^{\mathrm{T}}$. The surge velocity is set as $u_L=6\text{m/s}$ and the yaw angle is set as

$$r_L=\begin{cases}\exp\left(0.005t/300\right)\text{rad/s},\ t\le 30\text{s}\\ 0\,\text{rad/s},\ 30\text{s}<t\le 70\text{s}\\ 0.05\,\text{rad/s},\ t>70\text{s}\end{cases}\tag{58}$$

The ocean disturbances are established by $\boldsymbol{D}_w=\left[d_{wu},d_{wv},d_{wr}\right]^{\mathrm{T}}=\boldsymbol{d}_w+\boldsymbol{\omega}_w$, where

$$\boldsymbol{d}_w=\begin{cases}110\times\left(1+0.35\sin\left(0.2t\right)\right)\\ 260\times\left(1+0.3\cos\left(0.4t\right)+0.2\sin\left(0.1t\right)\right)\\ 950\left(1+0.3\cos\left(0.3t\right)+0.1\sin\left(0.5t\right)\right)\end{cases}\tag{59}$$

and $\boldsymbol{\omega}_w$ is generated by the first-order Markov process $\dot{\boldsymbol{\omega}}_w=-\Lambda\boldsymbol{\omega}_w+\Xi\aleph$, where $\aleph\in\mathbb{R}^3$ denotes the zero-mean Gaussian white noise.

4.1. Closed-loop performance

Consider one leader and four followers underactuated USVs. The objective of this task is to constitute a pentagon formation with model uncertainty and ocean disturbances. The leader-follower configuration constants are selected as: $\rho_{d1}=40\text{m}$, $\lambda_{d1}=7\pi/10\,\text{rad}$, $\rho_{d2}=40\text{m}$, $\lambda_{d2}=-7\pi/10\,\text{rad}$, $\rho_{d3}=45\text{m}$, $\lambda_{d3}=9\pi/10\,\text{rad}$, $\rho_{d4}=45\text{m}$, $\lambda_{d4}=-9\pi/10\,\text{rad}$. The initial states of the 4 virtual vessels are set as $\boldsymbol{\eta}_{\boldsymbol{v1}}=[-23\text{m},32\text{m},0\text{rad}]^{\mathrm{T}}$, $\boldsymbol{\upsilon}_{\boldsymbol{v1}}=[0\text{m/s},0\text{m/s},0\text{rad/s}]^{\mathrm{T}}$, $\boldsymbol{\eta}_{\boldsymbol{v2}}=[-23\text{m},-32\text{m},0\text{rad}]^{\mathrm{T}}$, $\boldsymbol{\upsilon}_{\boldsymbol{v2}}=[0\text{m/s},0\text{m/s},0\text{rad/s}]^{\mathrm{T}}$, $\boldsymbol{\eta}_{\boldsymbol{v3}}=[-42\text{m},3\text{m},0\text{rad}]^{\mathrm{T}}$, $\boldsymbol{\upsilon}_{\boldsymbol{v3}}=[0\text{m/s},0\text{m/s},0\text{rad/s}]^{\mathrm{T}}$, $\boldsymbol{\eta}_{\boldsymbol{v4}}=[-42\text{m},-25\text{m},0\text{rad}]^{\mathrm{T}}$, $\boldsymbol{\upsilon}_{\boldsymbol{v4}}=[0\text{m/s},0\text{m/s},0\text{rad/s}]^{\mathrm{T}}$. As for the follower USVs, the initial states are set as $\boldsymbol{\eta}_{\boldsymbol{1}}=[-23\text{m},32\text{m},0\text{rad}]^{\mathrm{T}}$, $\boldsymbol{\upsilon}_{\boldsymbol{1}}=[0\text{m/s},0\text{m/s},0\text{rad/s}]^{\mathrm{T}}$, $\boldsymbol{\eta}_2=[-23\text{m},-32\text{m},0\text{rad}]^{\mathrm{T}}$, $\boldsymbol{\upsilon}_2=[0\text{m/s},0\text{m/s},0\text{rad/s}]^{\mathrm{T}}$, $\boldsymbol{\eta}_3=[-42\text{m},3\text{m},0\text{rad}]^{\mathrm{T}}$, $\boldsymbol{\upsilon}_3=[0\text{m/s},0\text{m/s},0\text{rad/s}]^{\mathrm{T}}$, $\boldsymbol{\eta}_4=[-42\text{m},-20\text{m},0\text{rad}]^{\mathrm{T}}$, $\boldsymbol{\upsilon}_4=[0\text{m/s},0\text{m/s},0\text{rad/s}]^{\mathrm{T}}$. The main control parameters are set as $K_1=\text{diag}\left(5,1,6\right)$, $K_2=\text{diag}\left(1,1,6\right)$, $k_{x_1}=2$, $k_{x_2}=1$, $k_{y_1}=1.5\times10^7$, $k_{y_2}=4$, $k_{\psi_1}=82$, $k_{\psi_2}=4$, $k_{i1}=9\times10^4$, $k_{i2}=30$.

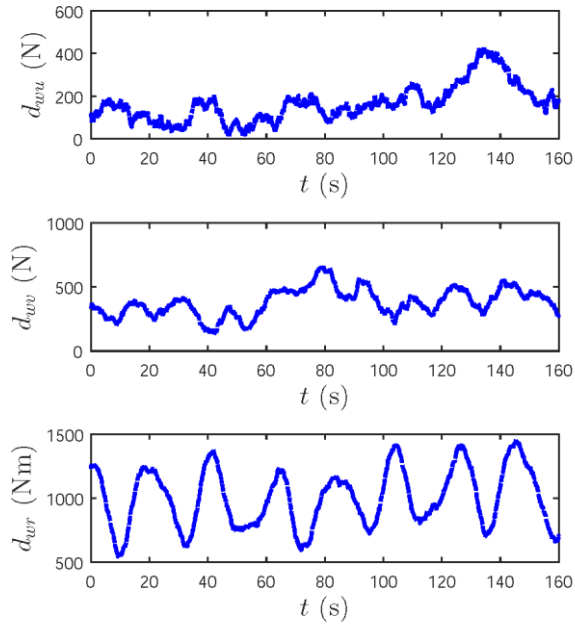

Fig.3 Forces and moments induced by ocean disturbances

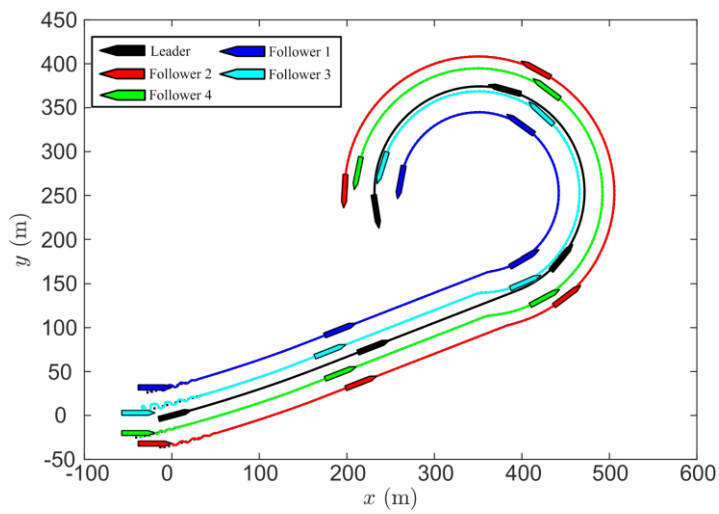

Fig.4 Trajectory of the leader-follower formation in the horizontal plane

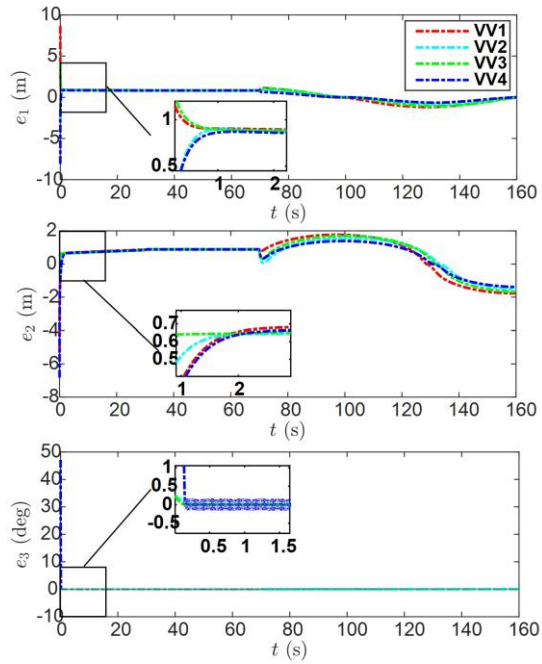

Fig.5 Position and orientation errors between the virtual vehicles and reference positions

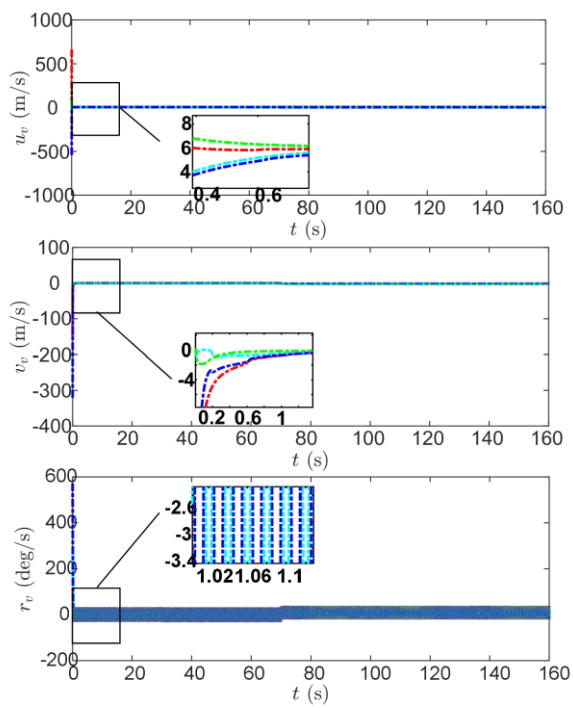

Fig.5 Surge, sway and yaw velocities of the 4 virtual vehicles

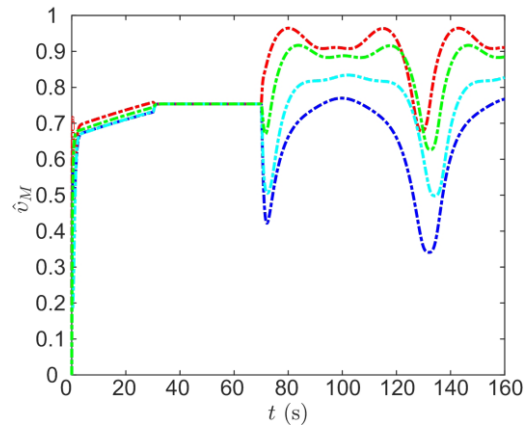

Fig.6 Adaptive parameters of the velocity controllers

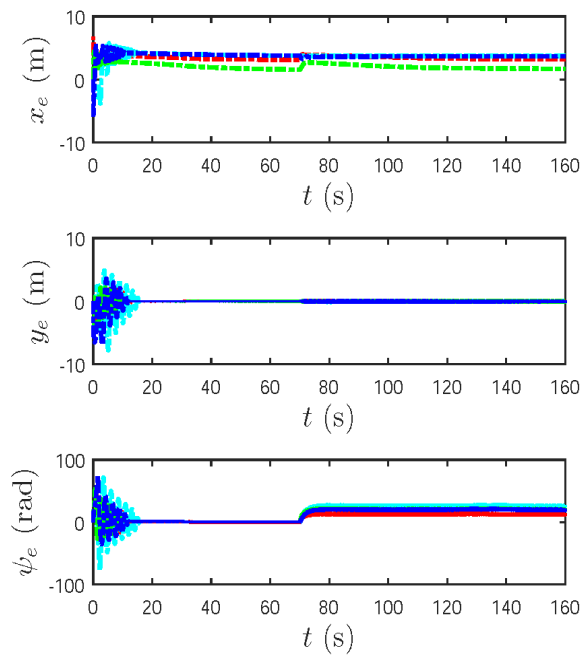

Fig.7 Position error between the 4 follower USVs and virtual vehicles

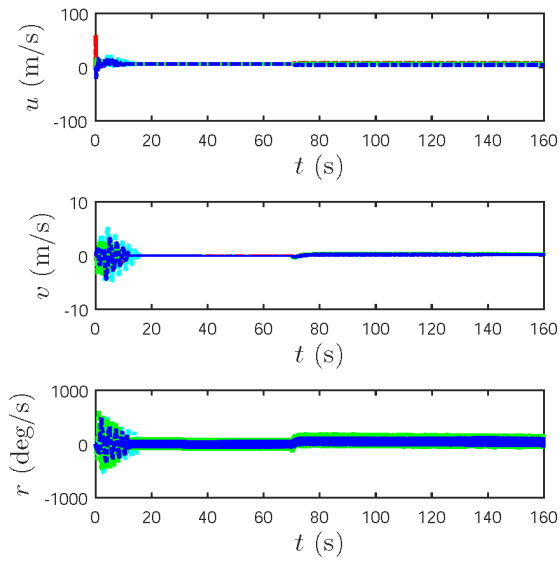

Fig.8 Surge, sway and yaw velocities of the 4 follower USVs

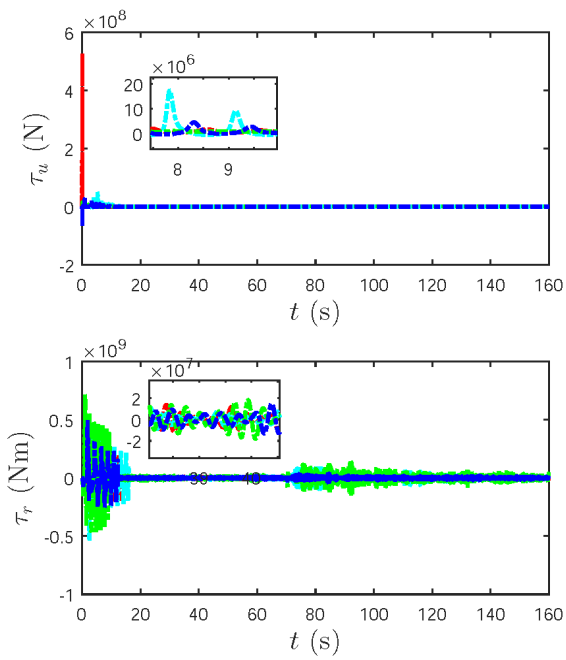

Fig.9 Control inputs of the 4 follower USVs in surge and yaw directions

Fig. 3~9 shows the simulation results of the proposed algorithm. Fig. 3 shows the forces and moment of the ocean disturbances acting on the follower USVs. From Fig. 4, it can be seen that the 4 follower USVs from random initial positions converge to their desired positions and finally constitute a pentagon formation with the leader USV, meanwhile, the formation remains undeformed despite moving on a curve path. Fig. 5 shows that the virtual vehicles (VVs) converge to their corresponding reference positions quickly and the tracking errors remain convergent after the leader USV turns at 70s. Fig. 6 shows that the surge, sway and yaw velocities of the virtual vehicles converge quickly. Fig. 6 shows the parameter adaptation result of the adaptive velocity control law. From Fig. 7, it can be seen that the position and yaw angle errors between the follower USVs and their corresponding virtual vehicles converge to a small residual set of origin in fixed time. Fig. 8 shows that the surge, sway and yaw velocities of the 4 follower USVs converge after a short period of adjustment. Fig. 9 shows the control inputs of the follower USVs in the surge direction and yaw direction.

4.2. Comparison example

In this task, the proposed controller is compared with the disturbance observer (DOB) based controller [32]. To compare the guidance principle and the control law more reasonably, only one single pair leader-follower is employed in the simulation. Select the desired distance and bearing angle between the leader and the reference position as $\rho_d = 40\text{m}$, $\lambda_d = -7\pi/10\,\text{rad}$. Select the initial condition $\boldsymbol{\eta}_{v1} = [-23\text{m}, 32\text{m}, 0\text{rad}]^{\mathrm{T}}$, $\boldsymbol{\upsilon}_{v1} = [0\,\text{m/s}, 0\,\text{m/s}, 0\text{rad/s}]^{\mathrm{T}}$ for the virtual vehicle and $\boldsymbol{\eta} = [-23\text{m}, 32\text{m}, 0\text{rad}]^{\mathrm{T}}, \boldsymbol{\upsilon} = [0\,\text{m/s}, 0\,\text{m/s}, 0\text{rad/s}]^{\mathrm{T}}$ for the follower. The main control parameters of the proposed controller remain unchanged.

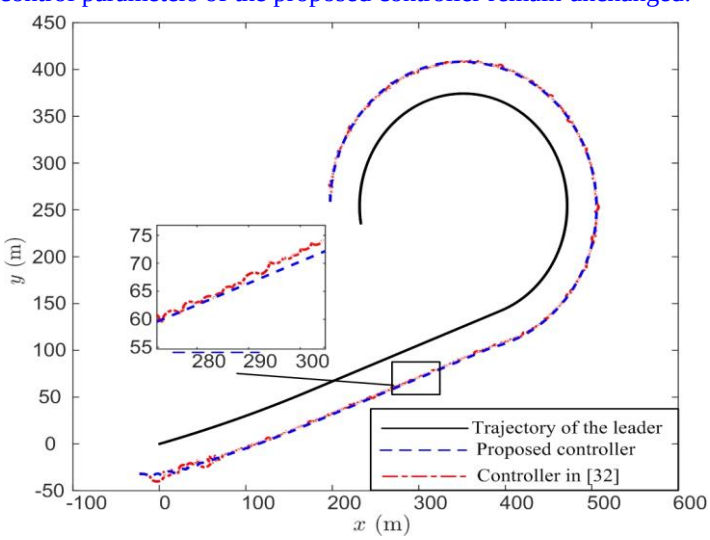

Fig.10 Comparison result of the USV trajectory

Fig.10~12 shows the comparison result of the proposed controller and the DOB-based controller in [32]. From Fig.10, we can learn that the follower is capable of tracking the reference position under both controllers. However, the proposed controller has a faster convergence rate and higher tracking accuracy. From Fig.11, it can be seen that the position errors between the virtual vehicle and the reference position can be stabilized quicker under the proposed leader-follower guidance principle. Fig.12 shows that the proposed controller is more robust with respect to ocean disturbances than the DOB-based controller.

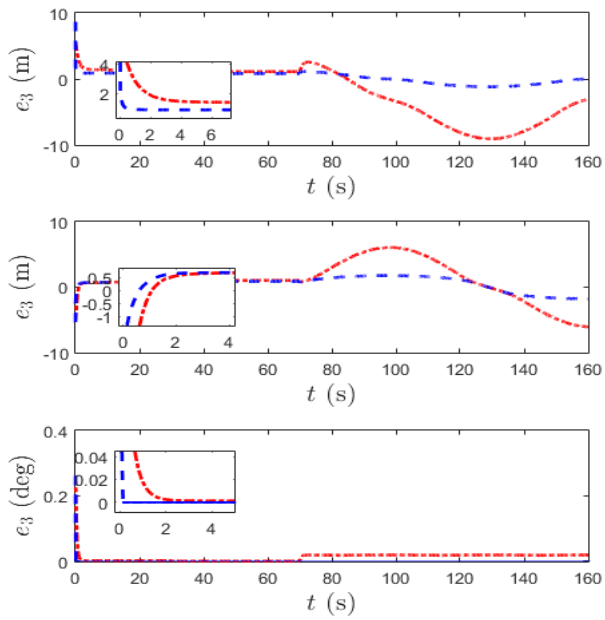

Fig.11 Comparison result of the errors between the virtual vehicle and the reference position

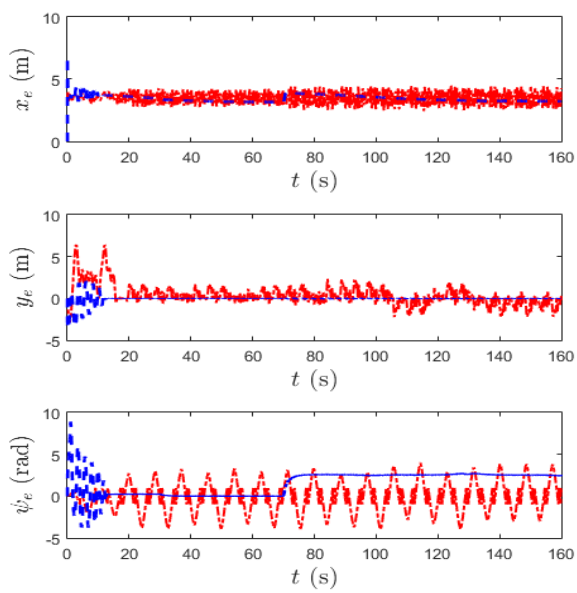

Fig.12 Comparison result of position error between the virtual vehicle and the follower USV

5. Conclusions

In this paper, a novel fixed-time sliding mode controller is presented for the formation control of underactuated USVs with unknown dynamics and ocean disturbances. To facilitate the leader-follower configuration, an adaptive fixed-time velocity controller is proposed for the virtual vehicles to enhance the guidance performance. For the tracking control of the follower USVs, the fraction power technique is introduced to modify the error signals of the controller to guarantee fixed-time convergence. An adaptive fixed-time filter is constructed to filter the virtual law to simplify the structure and reduce the computation burden of the proposed controller. By fusion of the RBFNN and bounded-feedback techniques, both the model uncertainty and the lumped disturbances of the USV are addressed effectively. Finally, numerical simulation is conducted to further verify the effectiveness of the presented algorithms. In the future, the problem of collision avoidance to dynamic and static obstacles by multi-USV will be investigated.

Acknowledgements

This work is partially supported by the Chinese Scholarship Council (No.202006570021), the National Natural Science Foundation of China (No. 51679024). This work contributes to the Strategic Research Plan of the Centre for Marine Technology and Ocean Engineering (CENTEC), which is financed by the Portuguese Foundation for Science and Technology (Fundação para a Ciência e Tecnologia - FCT) under contract UIDB/UIDP/00134/2020.

References

[1] G. Zhang, S. Liu, X. Zhang, W. Zhang. Event-triggered cooperative formation control for autonomous surface vehicles under the maritime search operation, IEEE Transactions on Intelligent Transportation Systems, 2022, DOI: 10.1109/TITS.2022.3181141.

[2] X. Zhan, Z. Guan, X. Zhang. F. Yuan. Optimal tracking performance and design of networked control systems with packet dropouts, Journal of the Franklin Institute, 2013, 350: 3205-3216.

[3] M.A. Hinostroza, H. Xu, C. Guedes Soares. Cooperative operative of autonomous surface vehicles for maintain formation complex environment. Ocean Engineering, 2019, 183: 132-154.

[4] M.A. Hinostroza, H. Xu, C. Guedes Soares. Experimental results of the cooperative operation of autonomous surface vehicles in complex marine environment. Ocean Engineering, 2021, 219: 108256.

[5] H. Xu, P. Oliveira, C. Guedes Soares. L1 adaptive backstepping control for path following of underactuated marine surface ships. European Journal of Control, 2021, 58: 357-372.

[6] H. Xu, T. I. Fossen, C. Guedes Soares. Uniformly semiglobally exponential stability of vector field guidance law and autopilot for path-following. European Journal of Control, 2020, 53: 88-97.

[7] D. Viegas, P. Batista, P. Oliveira, C. Silvestre. Decentralized state observer for range-based position and velocity estimation in acyclic formation with fixed topologies. Robust and Nonlinear Control, 2016, 5(26): 963-994.

[8] D. Viegas, P. Bastista, P. Oliveira, C. Silvestre. Discrete-time disturbance Kalman filter design for formations of autonomous vehicles. Control Engineering Practice, 2018, 75: 55-68.

[9] Å. Eek, K. Y. Pettersen, E. M. Rund, T. R. Krogstad. Formation path following control of underactuated USVs. European Journal of Control, 2021, 62: 171-184.

[10] G. Zhang, M. Yao, W Zhang, W. Zhang. Event-triggered distributed adaptive cooperative control for multiple dynamic positioning ships with actuator faults. Ocean Engineering, 2021, 242: 110124.

[11] Z. Tang, R. Cunha, T. Hamel, C. Silvestre. Some properties of time-varying bearing formation. European Journal of Control, 2022, doi: https://doi.org/10.1016/j.ejcon.2022.100699.

[12] J. Ghommam, M. H. Rahman, M. Saad. Design of distributed event-triggered circumnavigation control of a moving target by a group of underactuated surface vessels, European Journal of Control, 2022, 67: 100702.

[13] B.S. Park, S. J. Yoo. An error transformation approach for connectivity-preserving and collision-avoiding formation tracking of networked uncertain underactuated surface vessels. IEEE Transactions on Cybernetics, 2019, 49(8): 2955-2966.

[14] Z. Peng, D. Wang. Z. Chen, X. J. Hu, W. Y. Lan. Adaptive dynamic surface control for formation of autonomous surface vehicles with uncertain dynamics. IEEE Transactions on Control Systems Technology, 2012, 21(2): 513-520.

[15] R. Brooks. Robust layered control system for a mobile robot. IEEE Journal of Robotics and Automation, 1986, RA-2(1): 14-23.

[16] K. H. Tan, M. A. Lewis. Virtual structure for high-precision cooperative mobile robotic control. Proceedings of the International Conference on Intelligent Robots and Systems, Osaka, Japan: 1996.

[17] M. A. Lewis, K. H. Tan. High precision formation control of mobile robots using virtual structures. Autonomous Robots, 1997, 4: 287-403.

[18] J. Cruz. Leader-follower strategies for multilevel systems. IEEE Transactions on Automatic Control, 1978, 23(2): 244-255.

[19] M. Maghenem, A. Loria, E. Panteley. A robust δ-persistently exciting controller for leader-follower tracking-agreement of multiple vehicles. European Journal of Control, 2018, 40: 1-12.

[20] R. Yang, H. Zhang, H. Zhang. Event-triggered cooperative output regulation of heterogeneous multi-agent systems with switching topology. Acta Automatica Sinica. 2017, 43(3), 472-477.

[21] N. Wang, X. Li. Optimal output synchronization control of a class of complex dynamical networks with partially unknown system dynamics. IEEE Transactions on Systems, Man, and Cybernetics: Systems. 2021, 51(2), 822-832.

[22] A. Mousavi, K. Aryankia, R. R. Selmic. A distributed FDI cyber-attack detection in discrete-time nonlinear multi-agent systems using neural networks. European Journal of Control, 2022, DOI: https://doi.org/10.1016/j.ejcon.2022.100646.

[23] J. Ghommam, H, Mehrjerdi, M. Saad. Leader-follower based formation control of nonholonomic robots using the virtual vehicle approach, IEEE International Conference on Mechatronics, Istanbul, Turkey, 2011.

[24] J. Guo, Z. Lin, M. Cao, G. F. Yan. Adaptive leader-follower formation control for autonomous mobile robots. Proceedings of the American Control Conference, Baltimore, USA: 2010.

[25] S. Dai, S He, X. Chen, X. Jin. Adaptive leader-follower formation control of nonholonomic mobile robots with prescribed transient and steady-state performance. IEEE Transactions on Industrial Informatics, 2020, 16(6): 3662-3671.

[26] F. Fahimi. Sliding-mode formation control for underactuated surface vessels. IEEE Transactions on Robotics, 2007, 23(3): 617-622.

[27] R. Cui, S.S. Ge, B.V.E. How, Y. S. Choo. Leader-follower formation control of underactuated autonomous underwater vehicles. Ocean Engineering, 2010, 37(7), 1491-1502.

[28] X. Li, G. Yang. Neural-network-based adaptive decentralized fault-tolerant control for a class of interconnected nonlinear systems. IEEE Transactions on Neural Networks and Learning Systems, 2018, 29(1): 144-155.

[29] Z. Peng, D. Wang, X. Hu. Robust adaptive formation control of underactuated autonomous surface vehicles with uncertain dynamics. IET Control Theory and Application, 2011, 5(12): 1378-1387.

[30] K. Shojaei. Leader-follower formation control of underactuated autonomous marine surface vehicles with limited torque. Ocean Engineering, 2015, 105: 196-205.

[31] Z. Sun, G. Zhang, Y. Lu, W. D. Zhang. Leader-follower formation control of underactuated surface vehicles based on sliding mode control and parameter estimation. ISA Transactions, 2018, 72: 15-24.

[32] Y. Lu, G. Zhang, Z. Sun, W. D. Zhang. Robust adaptive formation control of underactuated autonomous surface vessels based on MLP and DOB. Nonlinear Dynamics, 2018, 94: 503-519.

[33] S. Dai, S. He, H Cai, C. G. Yang. Adaptive leader-follower formation control of underactuated surface vehicles with guaranteed performance. IEEE Transactions on Systems, Man, and Cybernetics: Systems, 2022, 52(3): 1997-2008.

[34] J. Xu. Formation tolerant finite-time leader-follower formation control for autonomous surface vessels with LOS range and angle constraints. Automatica, 2016, 68: 228-236.

[35] C. Huang, X. Zhang, G. Zhang. Adaptive neural finite-time formation control for multiple underactuated vessels with actuator faults. Ocean Engineering, 2021, 222: 108556.

[36] J. H. Li, P. M. Lee, B. H. Jun, Y. K. Lim. Point-to-point navigation of underactuated ships. Automatica, 2008, 44(12): 3201-3205.

[37] M. M. Polycarpou. Stable adaptive neural control scheme for nonlinear systems.IEEE Transactions on Automatic Control, 1996, 41(3): 447-451.

[38] B. Chen, X. P. Liu, K. Liu, C. Lin. Novel adaptive neural control design for nonlinear MIMO time-delay systems. Automatica, 2009, 45(6): 1554-1560.

[39] A. Polyakov. Nonlinear feedback design for fixed-time stabilization of linear control systems. IEEE Transactions on Automatic Control, 2011, 57(8): 2106-2110.

[40] M. M. Polycarpou, A. I. Petros, A robust adaptive nonlinear control design, American Control Conference, San Francisco, USA: 1993.

[41] M. Chen, H. Q. Wang, X. P. Liu. Adaptive fuzzy practical fixed-time tracking control of nonlinear systems. IEEE Transactions on Fuzzy Systems, 2021, 29(3):664-673.

[42] H. J. Yang, D, Ye. Adaptive fixed-time bipartite tracking consensus control for unknown nonlinear multi-agent systems: An information classification mechanism. Information Science, 2018, 459: 238-254.

[43] C. J. Qian, W. Lin. Non-Lipschitz continuous stabilizers for nonlinear systems with uncontrollable unstable linearization. Systems & Control Letters, 2001, 42(3): 185-200.

[44] N. Zhou, X. Cheng, Z. Sun, Y. Xia. Fixed-time cooperative behavioural control for networked autonomous agents with second-order nonlinear dynamics, IEEE Transactions on Cybernetics, 2021,DOI: 10.1109/TCYB.2021.3057219.